FEL SIMULATIONS WITH OCELOT

I. Agapov *, G. Geloni, European XFEL GmbH, Hamburg, Germany
S. Tomin, NRC Kurchatov Institute, Moscow, Russia, and European XFEL GmbH, Hamburg, Germany
M. Dohlus, I. Zagorodnov, DESY, Hamburg, Germany

Abstract

OCELOT has been developed as a multiphysics simulation tool for FEL and synchrotron light source studies. In this work we highlight recent code developments focusing on electron tracking in linacs taking into account collective effects and on x-ray optics calculations.

INTRODUCTION

OCELOT has been developed as a multiphysics python-based simulation and on-line control framework for free electron laser (FEL) and synchrotron light source studies. Overview of its design and application areas can be found e.g. in [1]. FEL simulations comprise electron beam dynamics, FEL process proper, and interaction of radiation with optics components. OCELOT is a framework to account for all such processes, by including native physics models or interfacing to third-party codes. FEL calculations heavily rely on *Genesis 1.3* [2], while for other physics processes native models of various complexity exist. In this work we focus on recent code developments in two application areas not discussed in [1]: electron beam dynamics with space charge effects and x-ray optics. Accounting for space charge effects is necessary to extend the application area to low energy electron transport. The other major physics process which has to be taken into account for electron beam dynamics in FELs is Coherent Synchrotron radiation (CSR). A corresponding solver for OCELOT is being introduced and will be discussed elsewhere. The x-ray optics module has been largely driven by the needs of self-seeded FEL and some crystal optics simulations. This paper discusses calculations of crystal reflectivity and transmissivity in the optics module. Ray tracing and Fourier optics methods have also been introduced but are not discussed here.

SPACE CHARGE EFFECTS

OCELOT has been recently extended for particle tracking with collective effects. A three-dimensional Poisson solver to take into account the space charge forces has been included. In the near future additional modules for coherent synchrotron radiation and wakefields will be included in the code as well. The tracking of particles is done in the same way as, for example, in Elegant [3]. Quadrupoles, dipoles, sextupoles, radiofrequency (RF) cavities and so on are modelled by linear or nonlinear maps. The focusing effect of RF cavities is taken into account according to [4]. The space charge forces are calculated by solving the Poisson equation in the bunch frame. Then the Lorentz transformed electromagnetic field is applied as a kick in the laboratory frame.

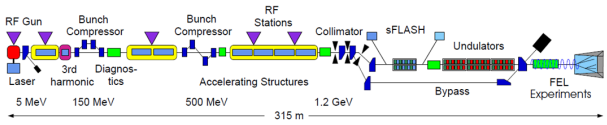

Figure 1: FLASH1 layout.

For the solution of the Poisson equation we use an integral representation of the electrostatic potential by convolution of the free-space Green's function with the charge distribution. The convolution equation is solved with the help of the Fast Fourier Transform (FFT). The same algorithm for solution of the 3D Poisson equation is used, for example, in ASTRA [5]. However, ASTRA solves equations of motion directly with a Runge-Kutta method, while in OCELOT particles are tracked using maps.

In this Section beam dynamics simulations for FLASH [6] using OCELOT are presented. FLASH is a high-gain FEL operating in the wavelength range of 4.2 - 45 nm. The layout of the facility is shown in Fig. 1. The formation of the electron bunch is carried out in two bunch compressors and seven TESLA-type 1.3 GHz superconducting accelerator modules. Each 12 m long module contains eight cavities. A special superconducting 3.9 GHz module built at FNAL has been installed in 2010 to improve the quality of the accelerated electron beam. The initial low-energetic part (14 meters from cathode of the gun) of the facility up to the third harmonic module was simulated with ASTRA since gun simulation is not presently possible in OCELOT. Then OCELOT was used to track the beam up to the entrance of the undulator section (203 meters from the cathode). The beam was tracked with and without taking space charge into account. The impact of space charge on the beam optics is shown in Fig. 2, where beta functions in the vertical plane without space charge (gray solid line) and with space charge (black points) are compared. A considerable mismatch is seen, which of course can be corrected. Such correction is not shown here since the focus is on benchmarking OCELOT with ASTRA.

The results of simulating the same setup with ASTRA is shown in Fig. 3. A slight disagreement between the two simulations is related to the fact that only first order maps were used for quadrupoles in OCELOT (higher order maps are presently used only for sextupoles and octupoles). This is also confirmed by cross-checks with Elegant. Higher order corrections to quadrupole and bending magnet maps are now being introduced in OCELOT as well. The current profile at the undulator entrance is shown in Fig. 4, where results obtained with OCELOT and ASTRA are compared.

* ilya.agapov@xfel.eu

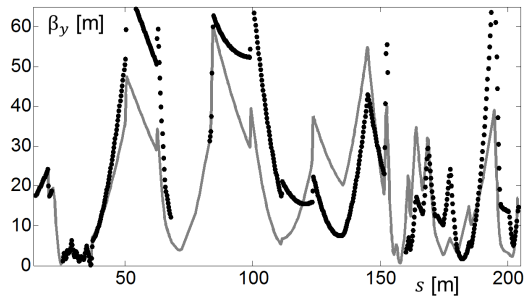

Figure 2: Vertical beta function with space charge (black points) and without (grey solid line) as obtained with OCELOT.

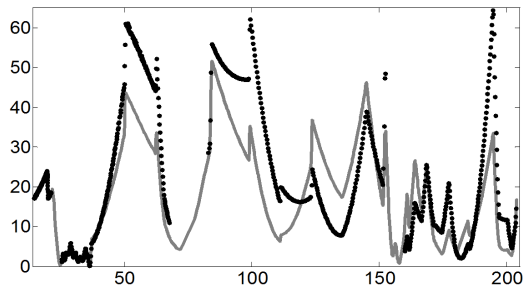

Figure 3: Vertical beta function with space charge (black points) and without (grey solid line) as obtained with ASTRA.

The difference is again due to using only linear optics in quadrupoles in OCELOT. The run time for OCELOT is significantly shorter than for ASTRA (few minutes compared to few hours on a PC).

X-RAY OPTICS MODULE

The optics module of OCELOT now includes the possibility of calculating reflectivity and transmissivity of perfect symmetric- or asymmetric-cut crystals using the dynamical theory of x-ray diffraction (see [7] for an authoritative textbook) in the two-beam case.

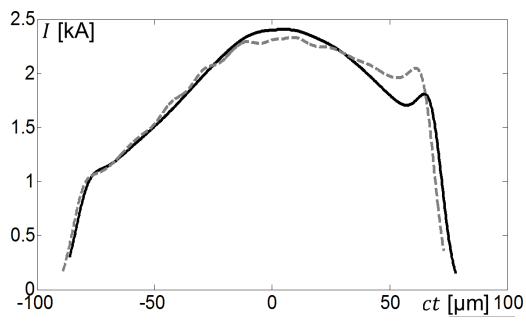

Figure 4: The current profile at the undulator entrance as obtained with ASTRA (solid black) and with OCELOT (grey dashed).

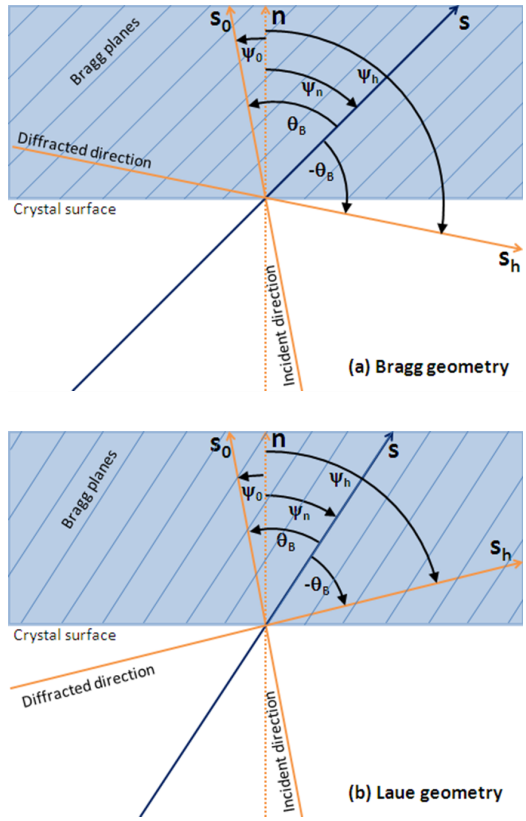

Figure 5: Sketch of (a) Bragg and (b) Laue scattering geometry.

The dynamical theory solves the problem of a monochromatic plane wave in a crystal. For such medium, the dielectric susceptibility can be expanded in Fourier series, due to the spatial periodicity of the electron density in the crystal, yielding

$$\chi(\vec{r}) = \sum_{\vec{h}} \chi_h \exp[-i\vec{h}\cdot\vec{r}]\,, \qquad (1)$$

with

$$\chi_h = -\frac{r_e \lambda^2 F_h}{\pi V_c}\,, \qquad (2)$$

where λ is the wavelength of interest, V_c the unit cell volume, r_e the classical electron radius and F_h the structure factor.

If one considers only the incident beam and one diffracted wave in the crystal, neglecting all other terms in the Fourier series, one remains with two beams. In this case, all possible wave vectors in the crystal are determined by two hyperboloid sheets in the reciprocal space. Boundary conditions for the electromagnetic field select the points on these sheets corresponding to the actual wave vectors in the crystals, and allow one to find transmissivity and reflectivity. Here we will

ISBN 978-3-95450-168-7

limit ourselves to describing the treatment implemented in OCELOT, without going into details concerning the theory of diffraction.

With reference to Fig.5, showing two generic examples for Bragg and Laue geometries, and following notation and conventions in [7] we indicate with $\vec{n}$ the unit vector normal to the crystal surface, directed inside the crystal, while the trace of the Bragg planes is indicated with the unit vector $\vec{s}$. The directions of incident and diffracted beams are specified, respectively, by the unit vectors $\vec{s}_0$, and $\vec{s}_h$. We call ψ_n the angle between $\vec{n}$ and $\vec{s}$, ψ_0 the angle between $\vec{n}$ and $\vec{s}_0$, and ψ_h the angle between $\vec{n}$ and $\vec{s}_h$. The signs of these angles are such that the Bragg angle θ_B between $\vec{s}$ and $\vec{s}_0$ is positive. We further define

$$\gamma_0 = \cos\psi_0\,, \quad \gamma_h = \cos\psi_h\,, \quad \gamma = \frac{\gamma_h}{\gamma_0} \tag{3}$$

so that $\gamma < 0$ in the case of Bragg scattering geometry, Fig. 5(a) and $\gamma > 0$ in the Laue scattering geometry, Fig. 5(b). We now set

$$\overline{PL} = \frac{\lambda\sqrt{\gamma_0|\gamma_h|}}{|C_p|\sqrt{\chi_h\bar{\chi}_h}} \tag{4}$$

$$\overline{MP}' = \frac{\chi_0}{2\lambda\gamma_0} + \mathrm{sign}(\gamma_h)\frac{\eta}{2\overline{PL}} - \frac{\sqrt{\eta^2+\mathrm{sign}(\gamma_h)}}{2\overline{PL}} \tag{5}$$

$$\overline{MP}'' = \frac{\chi_0}{2\lambda\gamma_0} + \mathrm{sign}(\gamma_h)\frac{\eta}{2\overline{PL}} + \frac{\sqrt{\eta^2+\mathrm{sign}(\gamma_h)}}{2\overline{PL}} \tag{6}$$

where the denominations $\overline{PL}$, $\overline{MP}'$ and $\overline{MP}''$ refer to the fact that these quantities are representative of segments in the reciprocal space [7]. The deviation parameter η is given by

$$\eta = \frac{\Delta\theta\sin(2\theta_B) + \chi_0(1-\gamma)/2}{\sqrt{|\gamma|}|C_p|\sqrt{\chi_h\bar{\chi}_h}}\,, \tag{7}$$

where $\Delta\theta = \theta - \theta_B$ indicates the angular deviation of the incidence angle from θ_B. Here it should be noted that reflectivity and transmissivity are invariant for transformations $\Delta\omega_B + \omega_B\Delta\theta\cot(\theta_B) = \mathrm{const}$, with $\Delta\omega = \omega - \omega_B$.

With these definitions, the transmissivity and reflectivity in the case of Bragg geometry is given by

$$T = \frac{(\xi' - \xi'')\exp[-2\pi i(\overline{MP}' + \overline{MP}'')\delta]}{\xi'\exp[-2i\pi\delta\overline{MP}'] - \xi''\exp[-2\pi i\delta\overline{MP}'']} \tag{8}$$

$$R = \xi'\xi''\frac{\exp[-2\pi i\delta\overline{MP}'] - \exp[-2\pi i\delta\overline{MP}'']}{\xi'\exp[-2\pi i\delta\overline{MP}'] - \xi''\exp[-2\pi i\delta\overline{MP}'']} \tag{9}$$

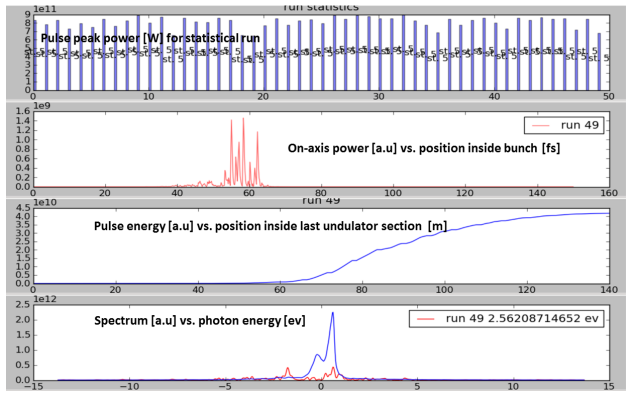

Figure 6: Screenshot of a hard x-ray self-seeding simulation for European XFEL with OCELOT.

where δ is the thickness of the crystal, the polarization factor C_p is given by $C_p = 1$ for σ-polarized light and $C_p = -\cos(2\theta_B)$ for π-polarized light, and

$$\xi' = -\frac{\mathrm{sign}(C_p)}{\sqrt{|\gamma|}}\frac{\sqrt{\chi_h\bar{\chi}_h}}{\bar{\chi}_h}\left(\eta + \sqrt{\eta^2-1}\right) \tag{10}$$

$$\xi'' = -\frac{\mathrm{sign}(C_p)}{\sqrt{|\gamma|}}\frac{\sqrt{\chi_h\bar{\chi}_h}}{\bar{\chi}_h}\left(\eta - \sqrt{\eta^2-1}\right) \tag{11}$$

Analogous expressions hold in the Laue case. Implementations of these expressions in the OCELOT package allow to combine x-ray beam generation studies with crystal optics, which is needed e.g. for self-seeding simulations (see Fig. 6), or for design of x-ray split-and-delay lines.

REFERENCES

[1] I. Agapov et al., "OCELOT: a software framework for synchrotron light source and FEL studies", Nucl. Instr. Meth. A. 768 (2014) pp. 151-156

[2] S. Reiche, "GENESIS 1.3: a fully 3D time-dependent FEL simulation code", Nucl. Instr. and Meth. A 429, 243, (1999)

[3] M. Borland, `http://www.aps.anl.gov/Accelerator_Systems_Division/Accelerator_Operations_Physics/software.shtml#elegant`

[4] J. Rosenzweig and L. Serafini, "Transverse particle motion in radio-frequency linear accelerators", Phys. Rev. E 49, 1599 (1994)

[5] K. Floettmann, `http://www.desy.de/~mpyflo/`

[6] `http://flash.desy.de/`

[7] A. Authier, Dynamical Theory of X-Ray Diffraction (Oxford University, 2001).